Journal of Volcanology and Geothermal Research 469 (2026) 108497

Contents lists available at ScienceDirect

Journal of Volcanology and Geothermal Research

journal homepage: www.journals.elsevier.com/journal-of-volcanology-and-geothermal-research

A classification scheme for olivine populations in the Upper Pleistocene to Holocene Igwisi Hills (Tanzania) kimberlite lavas and investigation of grain origins and evolution

J.J. Rawlings [a,b,*], T.M. Gernon [a], M.J. Stock [c], M.R. Palmer [a], C.M. Petrone [b], R.J. Brown [d], E. Humphreys-Williams [e]

[a] School of Ocean and Earth Sciences, University of Southampton, Waterfront Campus, European Way, Southampton, SO14 3ZH, Hampshire, United Kingdom
[b] Volcano Petrology Group, Natural History Museum London, Cromwell Road, London, SW7 5BD, United Kingdom
[c] Department of Geology, Trinity College Dublin, Dublin 2, Ireland
[d] Department of Earth Sciences, University of Durham, Arthur Holmes Building, Science Site, South Road, Durham, DH1 3LE, United Kingdom
[e] Department of Earth Sciences, University College London, 5 Gower Place, London, WC1E 6BS, United Kingdom

ARTICLE INFO

Keywords:
Olivine
Zoning
Forsterite
Mantle
Xenocryst
Kimberlite

ABSTRACT

Kimberlites are a class of alkaline igneous rock which sometimes contain diamonds and derive from mantle depths typically exceeding 150 km. We investigate the Upper Pleistocene to Holocene (12 ka) Igwisi Hills kimberlites to characterise the olivine grains and better understand their origins and evolution. We observe four distinct olivine populations. Macrocrysts are >1500 μm in diameter, rounded, monocrystalline grains with a Mg-rich xenocrystic core (Fo 90.5–92.8) and elevated Ni but depleted Ca and Mn contents, typical of granular mantle peridotite. Nodules are >1500 μm in diameter, rounded, polycrystalline grains with an Mg-rich core (Fo 91–92.4), also derived from granular peridotite. Microcryst grains are <1500 μm, subhedral-euhedral and can be subdivided into two types. Microcryst-a grains have a Mg-rich (Fo 90–92.5) xenocrystic core indicative of a mantle peridotite origin and microcryst-b grains have a Fe-rich (Fo 89–91) core that likely originated from disaggregated neoblasts. Olivine in all four populations displays four magmatic zones: internal zone, rim, rind and outermost rind, typical of kimberlites worldwide. Fe-rich internal zones are likely derived from a primitive kimberlite melt which entrained the cores. Mg-rich rims formed as the kimberlite melt evolved and crystallised around the internal zones. Fe-rich rinds formed as the kimberlite melt continued to ascend and further crystallised around the rims. Mg-rich outermost rinds crystallised from the kimberlite melt during the final stages of ascent. Based on these observations we present a new ascent model for the Igwisi Hills magmas.

1. Introduction

1.1. Kimberlite volcanology and petrology

Kimberlites are enigmatic, volatile rich, low viscosity igneous rocks that sometimes contain diamonds. Kimberlite magmas are sourced from mantle depths (>150 km) and ascend rapidly due to their high volatile contents (Sparks et al., 2006; Wilson and Head, 2007; Kjarsgaard et al., 2022; Gernon et al., 2023; Giuliani et al., 2023, 2025). Kimberlitic rocks are associated with small, monogenetic volcanoes, typically within 50-100 km wide clusters comprising tens of individual occurrences. Owing to their age and susceptibility to weathering, the surface expression of these volcanoes is typically absent, with kimberlites generally forming variously eroded intrusive, sub-surface pipe structures. They are typically only found on cratons where thick lithosphere extends to the mantle depths at which kimberlite magma exists (Clifford, 1966; Tappe et al., 2016; Pearson et al., 2021). In addition to their economic importance as the primary source of natural diamonds, the geochemistry of kimberlites allows us to examine the chemical and physical processes that occur within the deep lithosphere and asthenosphere (Giuliani et al., 2025). Nevertheless, many aspects of kimberlite formation, ascent and eruption remain poorly understood.

* Corresponding author at: School of Ocean and Earth Sciences, University of Southampton, Waterfront Campus, European Way, Southampton, SO14 3ZH, Hampshire, United Kingdom.
E-mail address: J.Rawlings@soton.ac.uk (J.J. Rawlings).

https://doi.org/10.1016/j.jvolgeores.2025.108497
Received 17 November 2025; Accepted 17 November 2025
Available online 21 November 2025

1.1.1. Olivine classification and origins in kimberlite

Kimberlites have a complex mineralogy due to the co-existence of entrained xenocrystic olivine originating from the mantle and magmatic olivine crystallised from the primary kimberlite melt, as well as other crustal and mantle xenoliths. The groundmass of kimberlites includes heavily serpentinised glass along with unique minerals such as monticellite, perovskite, apatite, phlogopite, spinel, zemkorite and calcite (Dawson, 1980; Mitchell, 1986; Golovin et al., 2017; Kjarsgaard et al., 2022). Early studies of olivine in kimberlites considered that entire grains were either xenocrystic or phenocrystic, with xenocrysts being derived from mantle peridotite wall rock during kimberlite ascent and phenocrysts being crystallised directly from the kimberlite magma (Mitchell, 1986). However, it is now recognized that most of the olivine grains from kimberlites have distinct zoning patterns with characteristic geochemical signatures pertaining to their origins. They feature a 'core' derived from mantle peridotite, often showing high Fo content and peridotite signature trace element patterns. We also observe a suite of Fe-rich cores which typically sample sheared peridotites or megacrysts (Howarth and Taylor, 2016; Giuliani, 2018; Soltys et al., 2020). These xenocrystic cores are often surrounded by an 'internal zone' formed from a primitive kimberlite melt. This zone is surrounded, in turn, by up to three zones formed directly from crystallisation of the evolved kimberlite magma, the first being a 'rim', surrounded by a 'rind' and occasionally an 'outermost rind' (Giuliani, 2018; Howarth and Gross, 2019; Abersteiner et al., 2020, 2022; Casetta et al., 2023).

We recognise the complications around naming conventions for olivine grains in kimberlites. In our study, we employ the terms used in Abersteiner et al. (2022), where 'macrocryst' describes the large, rounded, monocrystalline olivine grains and 'microcryst' describes the smaller, more euhedral, monocrystalline olivine grains. We also use the term 'nodule' to describe large, rounded polycrystalline olivine grains (Shaikh et al., 2021; Abersteiner et al., 2022).

1.2. Igwisi Hills Volcanoes geological background and previous studies

The Igwisi Hills volcanoes (IHV) are located in western Tanzania, (−4.887°S and 31.933°E) (Brown et al., 2012), on the ancient Tanzanian Craton, comprising Archean rocks >3 billion years old (Dawson, 2008). The average thickness of the crust on the Tanzanian Craton is 39 km (Baranov and Bobrov, 2018) and the thickness of the lithosphere on this craton varies from 150 to 250 km (Baranov and Bobrov, 2018; Gibson et al., 2013; Priestley et al., 2008; Wang et al., 2016). Lithospheric thickness in the IHV area is estimated at ~195 km according to the LithoRef model (Afonso et al., 2019) and geothermobarometry conducted by Shaikh et al. (2021) suggests an 180 km thick lithosphere beneath IHV.

The IHV consists of three small volcanoes: the Southwest Volcano, the Central Volcano and the Northeast volcano (Fig. 1). Cosmogenic ^{3}He dating reveals an age of 12.4 ±4.8 ka (Brown et al., 2012), making the IHV the youngest known kimberlites on the Earth, with the second youngest being the Kundelungu plateau pipes in the Democratic Republic of Congo, dated at 32.3 Ma (Batumike et al., 2008). Consequently, the Igwisi Hills kimberlites are relatively fresh and have not experienced significant post emplacement alteration (Brown et al., 2012; Brett et al., 2015), making them ideal for studying the petrology and geochemistry of kimberlite-type rocks.

The physical volcanology, petrology, mineralogy and geochemistry of the Igwisi Hills have been studied previously. Brown et al. (2012) mapped and dated the deposits and produced a detailed stratigraphy of the volcanoes. Early mineralogical studies in the 1950's recognized the unusual rounded shape of the olivine crystals, but there was much debate at this time as to whether or not these rocks were kimberlites given their unusual mineralogy (Fozzard, 1956; Bassett, 1954; Sampson, 1953). Further work by Dawson (1971) and Reid et al. (1975) revealed the presence of some of the minerals typically found in kimberlites, e.g. pyrope and Cr-diopside. Detailed studies of olivine grain morphology and implications for ascent processes in the Igwisi lavas have been conducted by Brett et al. (2015); Jones et al. (2014, 2019), who propose a rapid and turbulent ascent of these magmas, evidenced by features such as rounding attributed to particle-particle attrition.

Dawson (1994) and Willcox et al. (2015) provided the first comprehensive whole rock geochemistry data for Igwisi, as well as

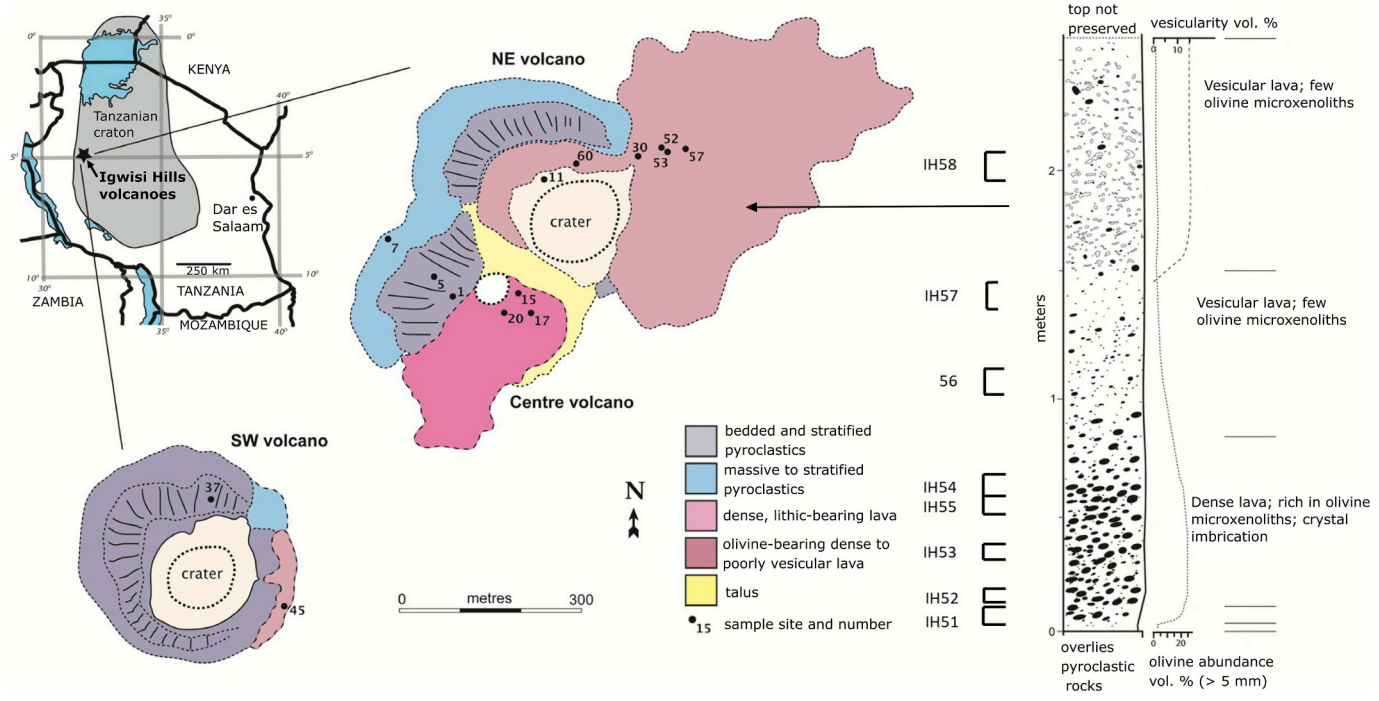

Fig. 1. Map showing the three volcanoes at Igwisi Hills, with inset to the left showing location of the Igwisi Hills volcanoes within the Tanzanian Craton. Inset to the right shows stratigraphic log of the olivine bearing lava flow of the Northeast (NE) volcano. Adapted from Brown et al. (2012) and Willcox et al. (2015). (For interpretation of the references to colour in this figure legend, the reader is referred to the web version of this article.)

petrological data. They also discovered new minerals not previously reported, such as a serpentine like mineral called 'Serpentine-X'.

Shaikh et al. (2021) also examined the geochemistry of the Igwisi lavas, with a particular focus on olivines, specifically 'dunitic nodules' which are large olivine grains (1-5 mm across) that feature small (<100 μm long axis) recrystallised olivines called 'neoblasts'. They use trace elements to determine their origins, and provide equilibration temperatures and pressures for cores of dunitic nodules. Shaikh et al. (2021) are the first to recognise zoning patterns in the IHV olivines, noting the presence of cores, internal zones and rims.

Our study builds on the work of Shaikh et al. (2021) which focuses primarily on the dunitic nodules in the IHV lavas. In contrast, our work focuses on olivine macrocrysts and microcrysts. By studying a larger number of these grains, taken from 8 units in the lavas of the Northeast volcano (Fig. 1), we report magmatic zonation in these macrocrysts and microcrysts that is more complex than previously thought. We document the presence of rinds and outermost rinds in these grains, as well as the cores, internal zones and rims observed by Shaikh et al. (2021). We also find that the microcrysts have two distinct core types, one being Mg-rich (90.5–92) and the other being Fe-rich (89–90.7) relative to their respective rim zones. Our work is important for understanding the evolution of the IHV magma and crystals within them, and the discovery of new zones may be useful for future applications such as diffusion chronometry, to provide constraints on the ascent rates of this exceptionally young and well preserved kimberlite.

2. Materials and methods

2.1. Sample suite

All samples used in this study were collected from the Northeast volcano's lava flow during fieldwork in 2010 and are detailed by Brown et al. (2012). Table 1 gives details of the samples, and these are mapped and plotted alongside a graphic log in Fig. 1. Samples were analysed in thin sections, with 11 sections in total used in this study.

2.2. Optical microscopy

Observations relating to the size, shape and textures of crystals were made using a Meiji optical microscope at the University of Southampton. Digital stitched images in both PPL and XPL were made of all sections using the Zeiss Axioscan 7 optical microscope at the Natural History Museum, London.

2.3. Scanning electron microscopy

The morphology, mineralogy, and zoning patterns of > 100 olivine crystals were examined in backscattered electron (BSE) images acquired using scanning electron microscopes (SEM). The FEI Quanta 650 field emission gun SEM at the Natural History Museum, London, was used to collect BSE images as well as compositional information over full thin sections, with a 7 μm pixel resolution, 25 kV accelerating voltage and 13 nA beam current. Data were analysed to produce phase maps of each thin section using the TESCAN Integrated Mineral Analyser (TIMA) software. A subset of crystals were imaged at higher resoluton with a 15 kV accelerating voltage, 100 nA beam current. Detailed BSE images and analyses of zoning patterns across individual olivine grains were also collected using a Carl Zeiss Leo 1450 variable pressure SEM at the University of Southampton, operating with a 20 kV accelerating voltage and 1.2 nA beam current.

Table 1
Table illustrating different levels within the Northeast lava flow that samples were collected from, by Brown et al. (2012).

Levels sampled in Northeast lava flow, Igwisi Hills volcanoes		
Sampling level	Height above base of flow (cm)	Description
IH58	195–205	vesicular olivine poor sample in zoned lava
IH57	135–145	olivine poor sample in zoned lava
IH56	100–110	olivine poor sample in zoned lava
IH55	60–70	transition zone between olivine rich and poor lava
IH54	53–60	top of olivine rich zone in zoned lava
IH53	30–43	olivine rich layer of zoned lava
IH52	15–20	slab and oriented sample of zoned lava
IH51	3–13	sample of zoned lava

2.4. Electron probe microanalysis

Transects were taken across olivine crystals of interest using a CAMECA SX100 electron probe micro analyser (EPMA) at the Natural History Museum, London. Major elements (Si, Fe, Mg) and trace elements (Ni, Mn, Al, Ca, Cr, P, Co) were measured simultaneously using five wavelength dispersive spectrometers (WDS). An accelerating voltage of 20 kV, beam current of 100 nA and beam diameter of 1 μm was used. Calibrations were conducted using international synthetic standard materials. Line transects were collected from the edge to the centre of crystals of interest, perpendicular to zoning, as recommended by Shea et al. (2015). Analysis points were taken every 5–10 μm along the transects to produce detailed profiles. When choosing locations for profiles, visible cracks and inclusions in olivines were avoided. When gathering transects across nodules (see 3.2.1 for description), care was taken to avoid areas with neoblasts (see 3.2.1 for description).

3. Results

3.1. General description of samples

In hand specimen, the most notable feature of these samples are the large (>1 mm) rounded olivines, set in a fine grained matrix. The only other discernible groundmass features visible with the naked eye are calcium carbonate laths (Fig. 2). When examining the samples under optical and scanning electron microscopes, we see many smaller olivines, ~90 % of which are <1 mm. BSE images also reveal that most olivines exhibit zoning, with crystals often having at least 2 zones (Figs. 3, 4 & 6). Microscopy also reveals abundant fine-grained groundmass minerals, such as calcite, chlorite, monticellite, spinel and apatite. Shearing in the olivines is also evident, in the form of kink banding and undulose extinction (Fig. 5b).

3.2. Morphology, mineralogy and zoning patterns in olivine

We can split the olivines into four main populations based on grain size, morphology, mineralogy and zoning patterns. Note, we follow the zone naming conventions of Abersteiner et al. (2022).

3.2.1. Macrocrysts and dunitic nodules

Macrocrysts have an ellipsoidal to rounded morphology and are generally large, with a long axis (i.e. length of crystal) range of 1–11 mm, and a mean long axis of 4.1 mm (Figs. 3 & 4). Macrocrysts typically show complex zoning patterns when viewed in BSE (Fig. 4), similar to zoning patterns observed in many kimberlite olivines worldwide (Brett et al., 2009; Howarth and Taylor, 2016; Lim et al., 2018; Giuliani, 2018; Soltys et al., 2018). They all have a core which is often rounded or embayed (Figs. 4a, c), although a minor amount (~5 %) are more euhedral (Fig. 4d). Cores range from 0.6 to 2.7 mm in diameter and sometimes contain pyrope, diopside, enstatite and phlogopite inclusions (Fig. 7). Inclusions in the cores can be large, with some enstatite crystals having long axes of >100 μm. Most macrocrysts have internal zones between the core and rim, which can appear rounded and slightly embayed, but much less so than the cores. The internal zones vary in

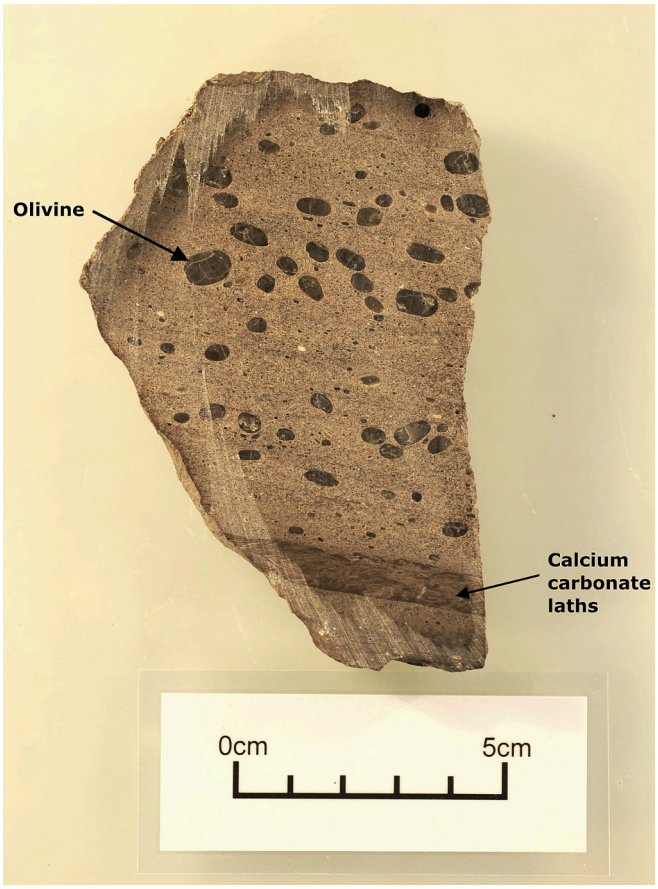

Fig. 2. Photograph of lava sample from the IHV Northeast volcano (sampling site IH51; see Fig. 1).

diameter (175–1240 μm wide) and contain abundant inclusions of Cr-spinel/chromite (Fig. 4c) and occasional phlogopite. Macrocrysts have mostly thin rims (~100 μm wide but some can be up to 250 μm). The macrocryst rims also contain inclusions of euhedral Cr-spinel. It is rare for rims to be complete around the macrocrysts; the rims are usually discontinuous/truncated in some areas and are often absent at the vertices of ellipsoidal grains. Some macrocrysts have thin, discontinuous rinds of 9–45 μm with Cr-spinel inclusions and a very few have thin, highly discontinuous outermost rinds (13–68 μm) with occasional Cr-spinel inclusions. The reader is directed to Fig. 3 for a schematic of representative crystals with labelled zones. Many macrocrysts contain thin (~10 um) fractures which can extend across all zones and have been filled with groundmass minerals such as monticellite, calcite and chlorite. Zoning is often asymmetrical in the macrocrysts, but there are a few examples of near symmetrical zoning (Fig. 4d). It is also important to note that not all macrocrysts preserve all 5 zones: there are a large number of crystals (~70 %) which only preserve cores, internal zones and rims, with a complete absence of rinds and outermost rinds.

Dunitic nodules are also present in the Igwisi Hills lavas, as first identified by Shaikh et al. (2021). The nodules have a largely similar morphology to the macrocrysts, but unlike macrocrysts, they are polycrystalline grains/aggregates, often comprised of several large olivine crystals and an abundance of much smaller olivine crystals called 'neoblasts' (Shaikh et al., 2021) with anhedral to subhedral habits (Fig. 5). Neoblasts are variable in size, from 80 to 200 μm, but the majority tend towards the lower end of this range. The nodules exhibit similar zoning patterns to macrocrysts, but the presence of all 5 zones is less common, and when present, this zoning is often interrupted by the occurance of chemically distinct neoblasts.

3.2.2. Microcrysts

The microcryst crystals are smaller than macrocryst crystals, the majority having a long-axis length <1500 μm (Figs. 3 & 6). They also show more variation in their morphology than macrocryst grains, with most grains being euhedral to subhedral, and a few exhibiting an anhedral morphology.

Microcryst crystals often show complex zoning patterns, similarly to macrocryst grains. Two types of microcryst cores exist. Microcryst-a cores are typically resorbed as indicated by their anhedral shapes and embayments, and contain mineral inclusions of enstatite. In contrast, microcryst-b cores are more euhedral-subhedral, also containing mineral inclusions such as enstatite. Both core types have similar diameters ranging from 200 to 450 μm. Where present, internal zones of microcryst grains are typically euhedral-subhedral, 70–120 μm in diameter and often contain inclusions of Cr-spinel, which in some grains are very abundant and seen in a distinctive, near-continuous ring within the zone (Fig. 6b). The rims of microcrysts are generally euhedral-subhedral, 30–80 μm in diameter and are often continuous around the crystal, containing inclusions of Cr-spinel. The rinds are euhedral, discontinuous and 10–60 μm in diameter. The outermost rinds are also euhedral, discontinuous and 10–20 μm in diameter. Again, like the macrocrysts, only around 20 % of microcrysts studied preserve rinds and outermost rinds. Zoning in the microcrysts is generally more symmetrical than in macrocrysts, but it is still uncommon to find perfectly symmetrical zones. An illustrative comparison between macrocrysts, nodules, microcryst-a and microcryst-b grains is provided in Fig. 3. The subpopulation of very small microcryst crystals (<500 μm) do not often show zoning and are occasionally anhedral. Accordingly, they are interpreted here as fragments of broken crystals from larger macrocryst and/or microcryst grains. Similarly to macrocryst grains, some microcrysts contain fractures extending across all the zones and have been filled with groundmass minerals such as monticellite, calcite and chlorite.

3.3. Olivine mineral chemistry

3.3.1. Macrocrysts and dunitic nodules

Forsterite contents of the measured macrocryst cores range from 90.1 to 92.4 ([Mg/(Mg + Fe) * 100] calculated using atomic % of Mg and Fe), with most tending towards the higher end of this range (Fig. 9). NiO contents of macrocryst and nodule cores are elevated at 0.27–0.42 wt%. MnO, CaO, Al_2O_3 and Cr_2O_3 in macrocryst and nodule cores are 0.088–0.110 wt%, 0.007–0.08 wt%, <0.01–0.021 wt% and <0.008 - 0.009 wt% respectively. Macrocryst and nodule internal zones have a restricted range of Fo contents of 89.5–90.4. NiO contents of internal zones are elevated compared to cores (0.30–0.49 wt%). MnO, CaO, Al_2O_3 and Cr_2O_3 in internal zones are 0.12–0.22 wt%, 0.04–0.29 wt%, <0.01–0.046 wt% and <0.008 - 0.052 wt% respectively. Rims of macrocrysts and nodules are Mg rich (Fo 90.7–92.2), with most rims at the higher end of this range. The rims are more invariable than core Fo. NiO contents of rims are variable (<0.009 - 0.37 wt%) but depleted compared to the cores. MnO, CaO, Al_2O_3 and Cr_2O_3 in rims are 0.14–0.33 wt%, 0.1–1 wt%, <0.01–0.035 wt% and 0.022–0.091 wt% respectively. Rinds often have a lower Fo content than their respective rims, with a range of 89.2–90.5. NiO contents are depleted (<0.009-0.18 wt%). MnO, CaO, Al_2O_3 and Cr_2O_3 in rinds are 0.2–0.25 wt%, 0.21–1.24 wt%, <0.01–0.025 wt% and <0.008-0.052 wt% respectively. In the few macrocryst and nodule grains where outermost rinds are present, they have typically very high Fo (90.8–93.2). NiO contents are heavily depleted (<0.009-0.058 wt%). MnO, CaO, Al_2O_3 and Cr_2O_3 in outermost rinds are 0.22–0.32 wt%, 0.25–0.57 wt%, <0.01–0.026 wt% and b.d.l. respectively. The reader is referred to Table 2 for a summary of macrocryst and nodule geochemistry, and Fig. 8a for a geochemical profile across a macrocryst grain.

Neoblasts within nodules have Fo ranging from 90.05–91.9, NiO contents of 0.22–0.38 wt%, CaO contents of 0.02–0.12 wt% and MnO

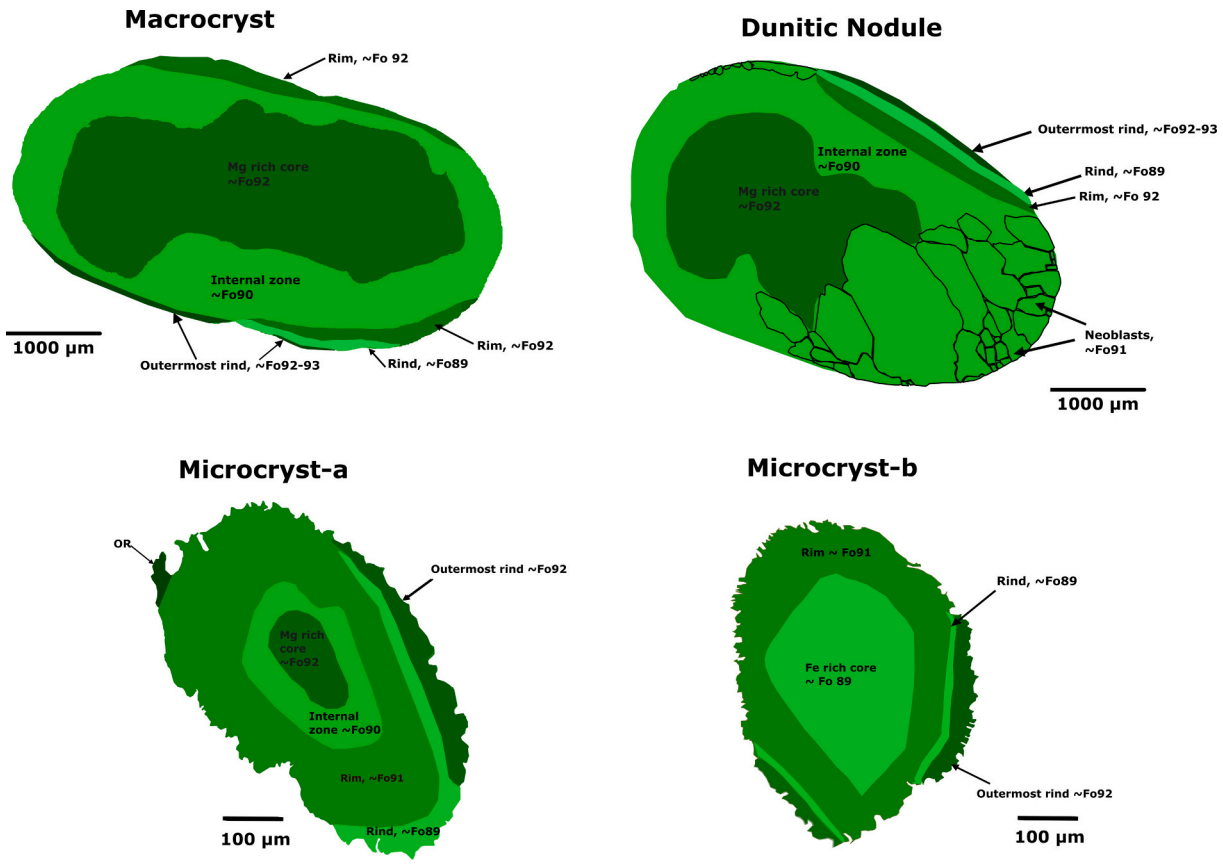

Fig. 3. Cartoon illustrating the morphology and zoning patterns in the four main olivine populations from the Igwisi Hills kimberlite lavas. IZ = internal zone. OR = outermost rind. Note these illustrations are based on real, SEM imaged crystals from the Igwisi lavas.

contents of 0.10–0.15 wt%, Al_2O_3 of <0.01-0.021 and Cr_2O_3 of 0.015–0.03 wt% (Supplementary Figs. 13–15). These neoblasts are unzoned.

We find our macrocrysts and dunitic nodule cores, internal zones and rims have a similar range in compositions to the respective zones in macrocrysts and nodules analysed in Shaikh et al. (2021) (see supplementary Figs. 2–12).

3.3.2. *Microcrysts*

As well as being morphologically distinct, microcryst-a and microcryst-b cores are geochemically distinct in their major oxides and forsterite contents. Microcryst-a cores are Mg-rich relative to their surrounding zone (internal zone or rim), typically having Fo contents of 90–92.5 (Fig. 10). They display a wide variation in NiO (0.1–0.39 wt%), have restricted and low MnO (0.10–0.14 wt%), low CaO (0.02–0.16 wt %), Al_2O_3 (<0.01–0.008 %) and Cr_2O_3 (<0.008- 0.045 wt%). Microcryst-b cores are Fe-rich relative to their surrounding zone, and have Fo contents of 89–91 (Fig. 9). NiO values are more restricted and elevated (0.33–0.46 wt%) compared to microcryst-a cores. Similarly to microcryst-a cores, microcryst-b cores have low MnO (0.11–0.13 wt%), CaO (0.04–0.12 wt%), Al_2O_3 (<0.01–0.016 wt%) and Cr_2O_3 (<0.008–0.059 wt%). Observations suggest that, out of all microcryst grains, ~70 % have Fe-rich cores relative to their rims (microcryst-b grains) and ~30 % have Mg-rich cores relative to their rims (microcryst-a grains). Internal zones of microcrysts have restricted and relatively low Fo contents (89.9–90.5) and low NiO contents of 0.29–0.47 wt%. MnO, CaO, Al_2O_3 and Cr_2O_3 in internal zones are all low at 0.11–0.16 wt%, 0.05–0.13 wt%, <0.01–0.017 wt% and <0.008–0.061 wt% respectively. It should be noted that microcryst-b grains often lack internal zones; these zones are much more ubiquitous in macrocrysts and microcryst-a grains. Rims of microcryst crystals have elevated Fo contents of 90.1–91.4 and a wide range of NiO contents (0.05–0.44 wt%). MnO, CaO, Al_2O_3 and Cr_2O_3 of rims are 0.13–0.29 wt%, 0.09–0.45 wt%, <0.01–0.037 wt% and <0.008–0.079 wt% respectively. Rinds have low Fo contents (89.2–90.6) and low NiO (0.02–0.18 wt%). MnO, CaO, Al_2O_3 and Cr_2O_3 of rinds are 0.12–0.26 wt%, 0.17–0.34 wt%, <0.01–0.06 wt% and <0.008–0.034 wt% respectively. Outermost rinds have elevated Fo contents (90.5–93.2), with most tending towards the higher end of this range, and have low NiO (0.009–0.05 wt%). MnO, CaO, Al_2O_3 and Cr_2O_3 of outermost rinds are 0.03–0.28 %, 0.25–0.95 wt %, 0.018–0.312 wt% and <0.008–0.008 wt% respectively. The reader is referred to Table 3 for summary of microcryst geochemistry. We note that the geochemistry of internal zones, rims, rind and outermost rinds is very similar for microcryst-a and microcryst-b grains. The reader is referred to Figs. 8b and c for examples of profiles across these grains. Further, we find the phenocrysts analysed in Shaikh et al. (2021) show largely similar compositions to our microcryst cores.

4. Discussion

4.1. *Magma evolution and petrogenesis of Igwisi olivines*

4.1.1. *Origins of cores*

Cores of the macrocrysts, nodules and microcryst-a crystals have elevated Fo and NiO, but low CaO and MnO, typical of cratonic mantle derived peridotitic olivine (Arndt et al., 2010; Shaikh et al., 2021; Abersteiner et al., 2022). Furthermore, low CaO contents have been suggested to provide evidence of crystallisation at high pressures (Simkin and Smith, 1970). These core zones also contain inclusionsof mantle minerals such as pyrope, enstatite and diopside. Together, these data suggest that the cores in IHV olivines are xenocrystic and mantle-derived, likely granular peridotites (Fig. 9). Populations of granular

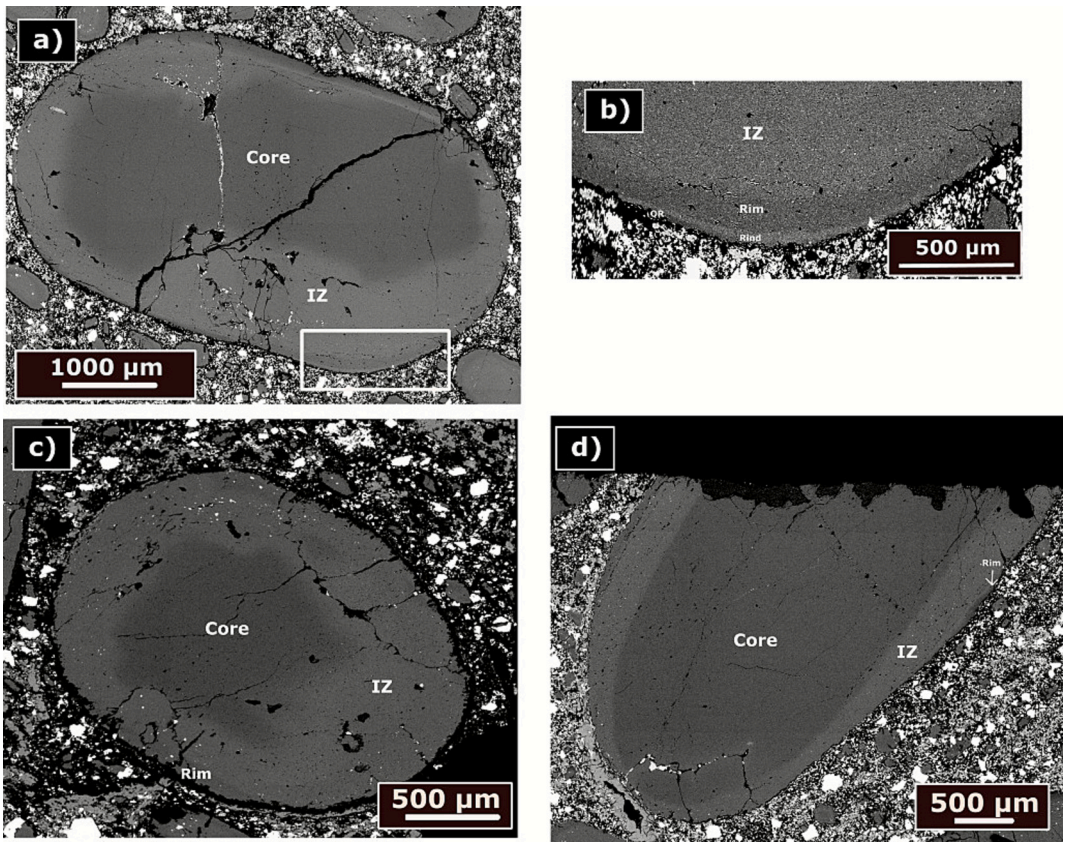

Fig. 4. BSE SEM images of olivine macrocrysts from the IHV lavas. Panel a) illustrates a particularly large grain featuring a core, internal zone (IZ), rim, rind and outermost rind (OR). Panel b) shows a close up of the area within the white box of panel a). Here we see a close up view of the internal zone, rim, rind and outermost rind. Panel c) shows an macrocryst grain with a core, internal zone and rim. Panel d) shows a rare macrocryst with a less resorbed core, also featuring an internal zone and rim.

peridotite derived cores are found in olivines from kimberlites worldwide (Brett et al., 2009; Lim et al., 2018; Giuliani, 2018; Kamenetsky et al., 2008; Abersteiner et al., 2020). For example, at Udachnaya-East, Siberia, a population of olivine cores with Fo 90.5–94 are observed and attributed to a granular peridotite origin (Casetta et al., 2023). Many olivine cores from the Kimberley kimberlite, South Africa, and Lac de Gras, Canada are also Mg enriched with low CaO and plot within granular peridotite fields (Giuliani, 2018) (see Fig. 9).

Cores of macrocrysts, nodules and microcryst-a crystals are typically highly resorbed (Figs. 4a, c, 6a and b) indicating they were in chemical disequilibrium with the surrounding melt (again attesting to their xenocrystic origin), resulting in dissolution of the outer portions of the core into the melt. Microcryst-a cores, which are similar in composition to those of macrocrysts, likely come from smaller and/or broken granular peridotite crystals due to their much smaller diameters. The Fo content of microcryst-b cores is towards the lower end of the range expected for granular mantle peridotites (De Hoog et al., 2010; Tomlinson and Kamber, 2021). Microcryst-b cores could represent sheared mantle peridotites from a dense thermal boundary layer as is the case with other kimberlite olivines with low Fo, sheared cores particularly in those from southern Africa (Gernon et al., 2023; Baptiste et al., 2012). However, shearing in the IHV olivines is not exclusive to microcryst-b crystals. Shearing textures such as undulose extinction and kink banding are also observed in macrocrysts, nodules and microcryst-a grains. Also, shearing does not appear to be exclusive to the core zones of the olivines. These factors make it unlikely that microcryst-b cores are sheared mantle peridotites. An alternative explanation is that these low Fo cores originate from a megacryst suite. Moore and Costin (2016) suggested that some of the olivine grains from Igwisi may be derived from Cr-rich megacrysts. The authors noted similarity in grain morphology and some trace oxides (e.g. TiO_2) and in the chemical composition of their clinopyroxene and garnet inclusions to Cr-rich megacrysts. However, we consider this unlikely due to the small size of microcryst-b cores compared to megacrysts. Megacrysts are typically >1 cm (Schulze, 1984; Nkere et al., 2021), whereas these cores typically have diameters of <500 um. Kimberlite melts can entrain large megacryst cores which are later reduced to smaller sizes due to dissolution and mechanical abrasion during ascent (Jones et al., 2014, 2019). However, due to the euhedral-subhedral shape of the cores it is unlikely that they represent fragments of broken megacrysts. Furthermore, they do not plot within the megacryst geochemical fields (Fig. 9). Another possibility is that microcryst-b cores originate from the neoblasts commonly found in nodules. These neoblasts are exclusive to the internal zones of nodules at the IHV (Shaikh et al., 2021) which have a low Fo content. These neoblasts could become disaggregated from their host nodules during a rapid ascent. We find that microcryst-b cores and neoblasts in Igwisi olivines have elevated trace element concentrations (e.g., Al, Ti and Ca) compared to macrocryst and microcryst-a cores, and similar euhedral morphologies, providing evidence that the microcryst-b cores may be neoblasts derived from granular peridotite nodules. Furthermore, neoblasts and microcryst-b cores have similar NiO, MnO and CaO contents (Supplementary Figs. 13–15). It is thought that such neoblasts can form by fluid or melt (enriched in CO_2 and H_2O) assisted recrystallisation and annealing of mantle peridotites after deformation (Shaikh et al., 2021). Similar low Fo cores derived from neoblasts have been reported in other kimberlites, for instance in the Kimberley kimberlites, South Africa (Soltys et al., 2020).

A notable difference between the IHV olivine cores and those from kimberlites worldwide is the Fo ranges of the cores. The IHV olivine cores (Fo 89–92.5) appear to have a relatively restricted range of Fo

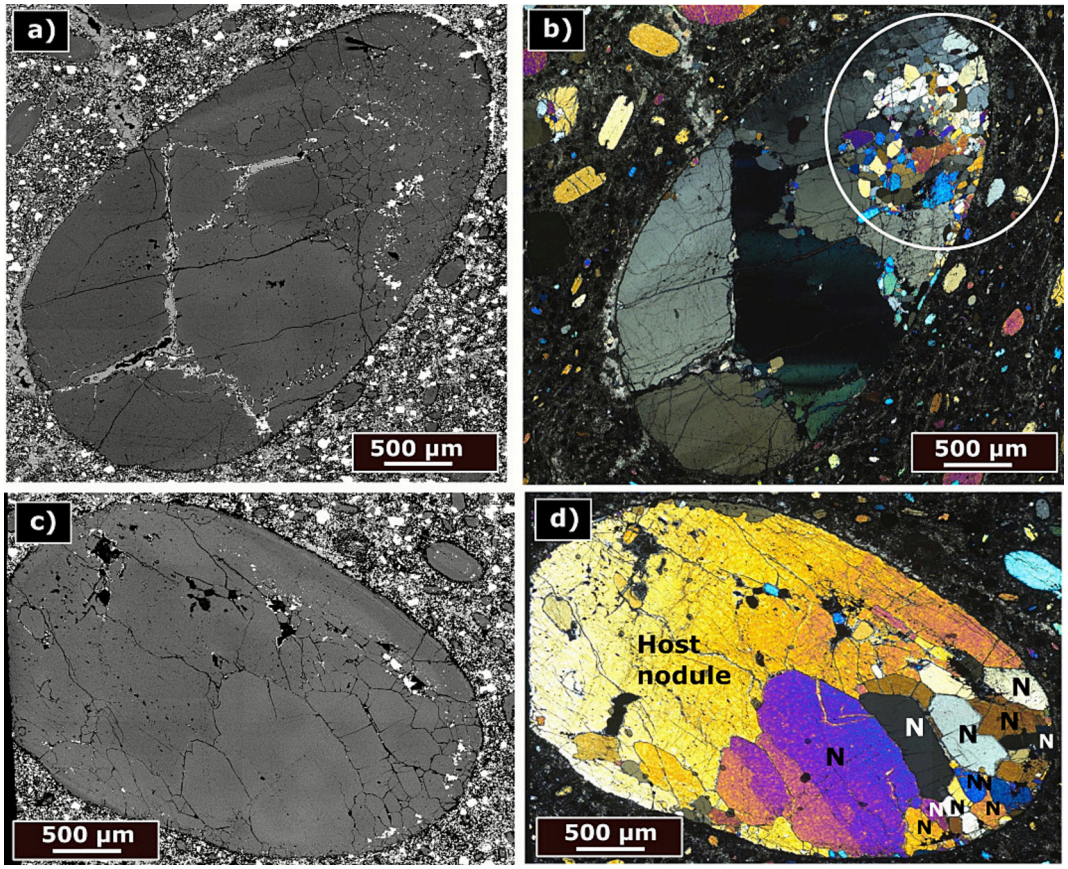

Fig. 5. BSE images and photomicrographs illustrating dunitic nodules from the Igwisi Hills lavas, with neoblasts labelled 'N'. Panel a) is an BSE image of a nodule. Panel b) is an optical microscope image taken under crossed polarised light of the same nodule in panel a). Note the encircled area in panel b) highlights a cluster of many small neoblasts. Panel c) shows another example of a nodule taken using BSE imaging. Panel d) shows the same nodule as in panel c) but under crossed polarised light using an optical microscope.

compared to kimberlites globally, e.g. the Udachnaya kimberlites mentioned above where several core populations exist, ranging from Fo 85–94. The Fe-rich cores (<Fo 89) seen in many kimberlites worldwide are derived from megacrysts or sheared peridotites, which are often affected by metasomatism. The lack of Fe-rich cores at IHV may indicate that metasomatism does not dominate here to the same extent as other kimberlite localities. The restricted and relatively high Fo contents seen in peridotite cores from IHV may also be indicative of sampling from a refractory sub-continental lithospheric mantle, as seen in other kimberlites such as Lac De Gras (Bussweiler et al., 2015; Tovey et al., 2022). Gibson et al. (2013) also propose a highly refractory lithospheric mantle exists beneath the Tanzanian craton based on the geochemistry of peridotites from the Lashaine tuff cone in northern Tanzania.

4.1.2. Origins of internal zones

The magmatic Cr-spinel and lack of mantle derived mineral inclusions (e.g. enstatite, diopside) in the internal zones provides evidence of their magmatic origin. Cr-spinel is one of the first minerals to crystallise from kimberlite melts (Soltys et al., 2018; Mitchell et al., 2019), suggesting a highly primitive kimberlite melt at IHV may have reacted with the outer region of the cores and crystallised around them to form the internal zone. We propose that such a primitive kimberlite melt would have formed by the early evolution of a proto-kimberlite melt. The proto-kimberlite melt was likely a carbonate-rich silicate melt with high Mg and Ca, and low Al, that initially did not have sufficient silica to crystallise olivine, but assimilates orthopyroxene and clinopyroxene during ascent, resulting in subsequent olivine crystallisation forming the internal zones (Giuliani et al., 2023, 2025). Furthermore, a primitive kimberlite melt would likely have been Mg-rich but relatively Fo depleted, Si-poor and Ca-rich compared to mantle derived perioditic cores (Abersteiner et al., 2022), trends which we observe in our grains. Alternatively, the low Fo contents of the internal zones may suggest they crystallised from a previous pulse of kimberlite melt that had undergone fractionation as has been suggested for internal zones in other kimberlites (Lim et al., 2018). However, we conclude that the internal zone is derived from crystallisation of a primitive kimberlite melt due to similarities in composition to an early kimberlite melt and the presence of key indicator minerals such as Cr-spinel. Internal zones are seen in some kimberlites from around the world, for example Casetta et al. (2023a) identify them in the Udachnaya-East kimberlites (Fo 85–87) and Soltys et al. (2020) note their presence in the De Beers pipe, Kimberley (Fo 89.2–91). The differances in Fo between these internal zones of kimberlites worldwide is likely due to the effects of assimilation, with the early kimberlite magma often being chemically altered by products it assimilates during its ascent (i.e. wall rocks), which will vary compositionally at each locality (Dalton et al., 2020; Giuliani et al., 2020).

4.1.3. Origins of rims, rinds and outermost rinds

The rims in all types of olivine in the IHV lavas have restricted Fo contents, low NiO, and elevated CaO and MnO contents. This observation, along with their euhedral-subhedral habits, supports a late stage crystallisation origin (Fedortchouk and Canil, 2004). Additionally, there is a lack of typical mantle-derived mineral inclusions, e.g., enstatite and pyrope, in the rim zones and we instead see magmatic phases such as Cr-spinel. A magmatic origin has also been suggested for many olivine rims of kimberlites globally, which show similar features to the IHV olivine rims (Brett et al., 2009; Giuliani, 2018; Abersteiner et al., 2020; Soltys et al., 2020). We therefore infer that the rims of olivines in the IHV are

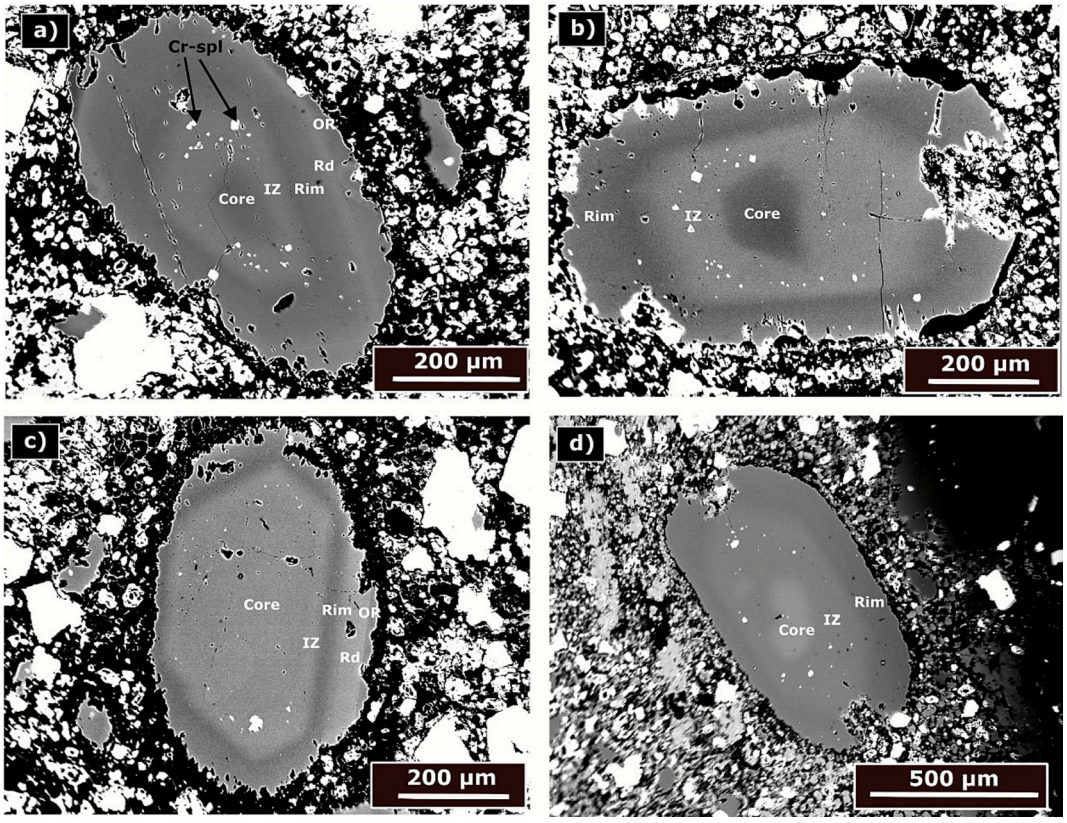

Fig. 6. BSE SEM images of olivine microcrysts from the IHV lavas. Panels a) and b) show microcryst-a grains (Mg-rich cores) and panels c) and d) show microcryst-b grains (Fe-rich cores). IZ = internal zone. Rd = rind. OR = outermost rind. Cr-spl = chrome-spinel.

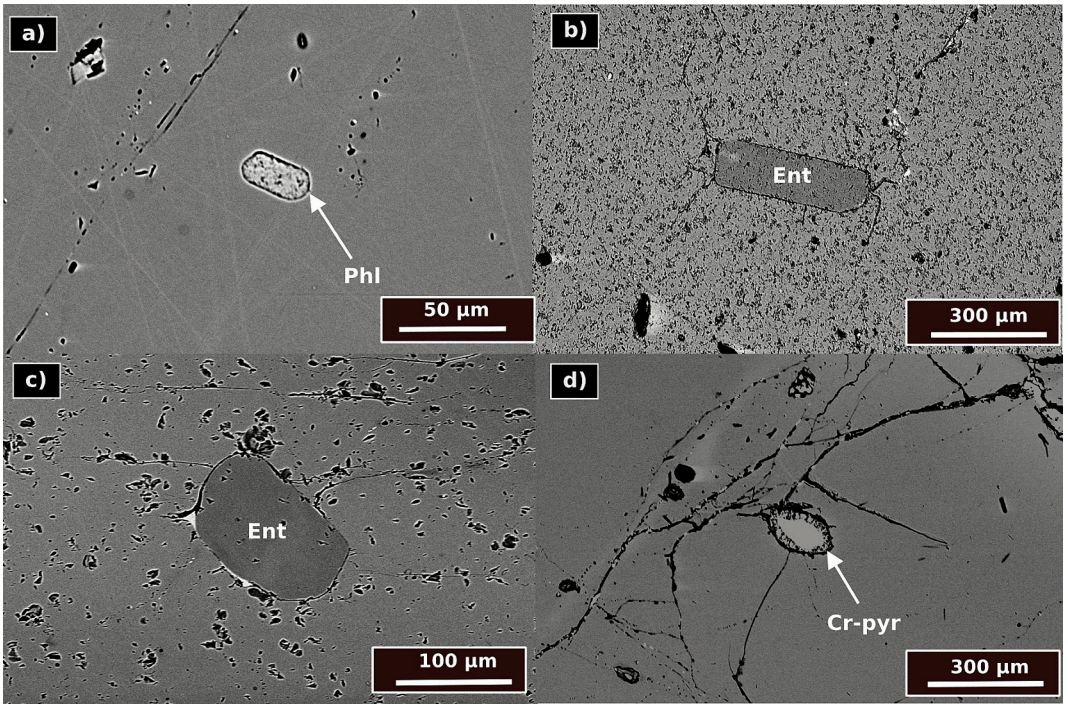

Fig. 7. BSE SEM images illustrating inclusions seen in cores of both macrocryst and microcryst crystals from the Igwisi Hills lavas. Panel a) shows a phlogopite crystal inclusion observed in the core of a microcryst-b grain. Panel b) shows an enstatite crystal inclusion observed in the core of a microcryst-a grain. Panel c) shows an enstatite crystal inclusion in the core of a macrocryst grain. Panel d) shows a chrome-pyrope crystal inclusion in the core of a macrocryst grain. Phl = phlogopite, Ent = enstatite, Cr-pyr = chrome-pyrope.

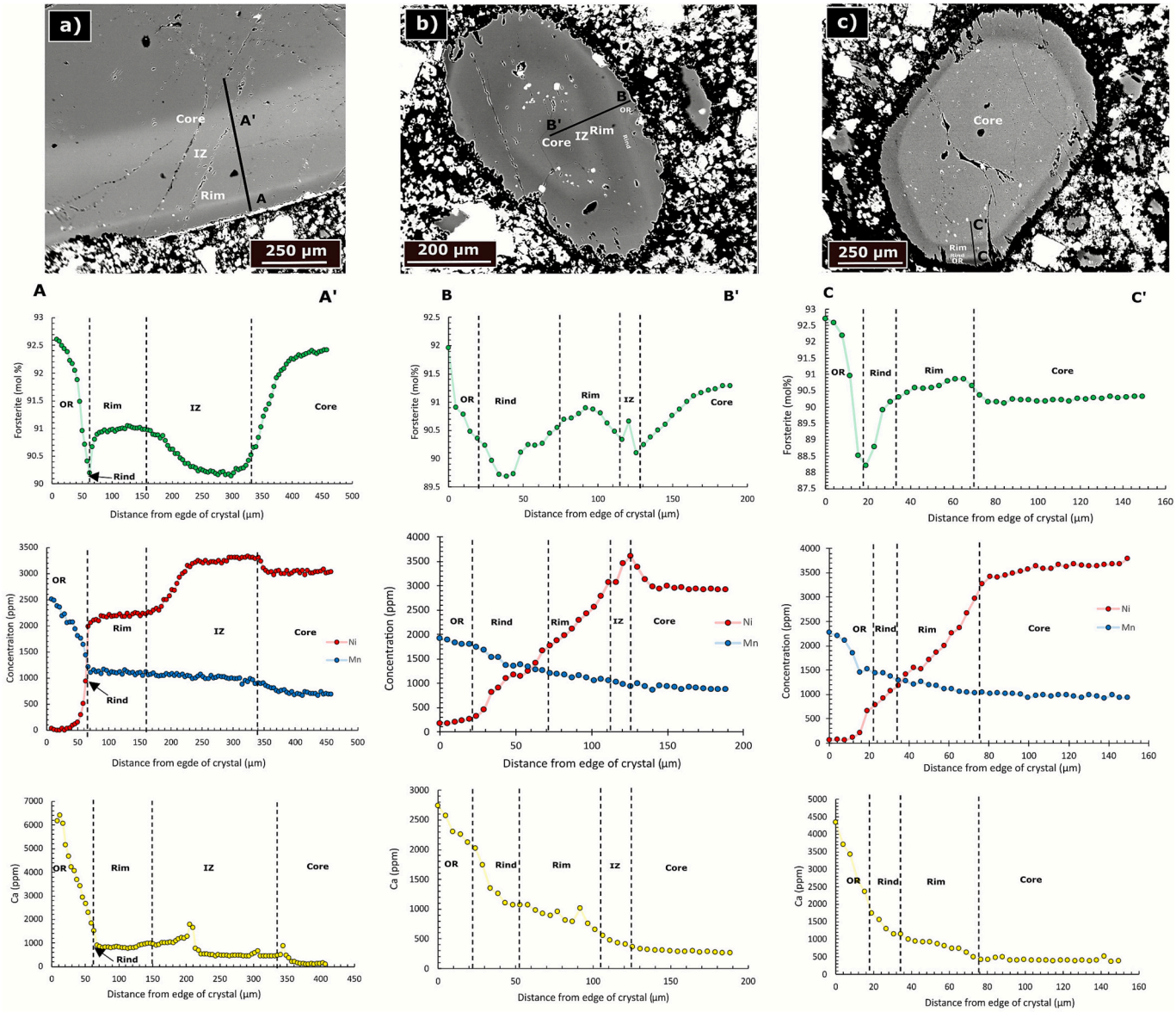

Fig. 8. Geochemical profiles across olivine grains from the IHV lavas. Each panel shows a BSE image (with zones and transect location labelled) and profiles for Fo, Ni, Mn and Ca. Panel a) shows data for a macrocryst grain, b) a microcryst-a grain and c) a microcryst-b grain.

magmatic in origin and crystallised from the evolved host kimberlite melt. Geochemistry of olivine rims worldwide can vary, again a reflection of processes such as assimilation during ascent of the kimberlite melt, with rims in the Mark kimberlite, Lac de Gras reaching Fo 97 and rims in the Udachnaya-East kimberlites, Siberia, having Fo as low as 88.6.

The rinds are also likely to be magmatic rather than mantle derived, evidenced by their even lower NiO and greater CaO and MnO contents relative to the cores (with CaO being particularly high), and the similar lack of mantle-derived mineral inclusions. We also note the ubiquitous decrease in Fo in the rinds of these olivines compared to their respective rims. Many kimberlites globally show an increase in Fo in the rind (Giuliani, 2018; Lim et al., 2018), for instance the Kimberley olivines which have Fo reaching 92.6 (Soltys et al., 2020) and the Lac de Gras olivines which have rinds of up to Fo 98 (Abersteiner et al., 2020). The IHV olivine rinds may be comparatively low in Fo due to late stage crystallisation within the lithosphere from a Mg—Ni depleted kimberlitic melt which previously crystallised an abundance of olivine and spinel.

The outermost rinds show very high Fo, interpreted to be caused by an increase in oxygen fugacity as the melt evolves and ascends closer to the surface, causing crystallisation of Fe-rich spinel, as seen in other kimberlite olivines, such as those from the Kimberely cluster (Soltys et al., 2018). The increase in Fo could also be due to recharge from a more primitive magma. While kimberlite eruptions are not fed from a conventional magma chamber/reservoir system, a single kimberlite body can be formed from multiple pulses of kimberlite magma (Scott Smith et al., 2013), as evidenced by chemical zoning (Sparks, 2013). However, we note that NiO is lowest in outermost rinds, low NiO being a feature typical of late-stage kimberlite magma crystallisation, suggesting it is unlikely a new pulse of kimberlite magma was involved in the formation of outermost rinds. A magma recharge event would also not be consistent with the relatively large range in Fo seen in our outermost rinds (Fig. 10). Outermost rinds are rare in kimberlites worldwide but have been seen in olivines from the Lac De Gras field. However, these are more Mg-rich than the outermost rinds seen at IHV, with Fo contents of 93–95 (Fig. 9) (Abersteiner et al., 2020) which likely reflects their assimilation of more Mg-rich material or a more marked change in oxygen fugacity during the late-stage ascent (Giuliani, 2018).

Supplementary Fig. 8 shows the large range of CaO values for the

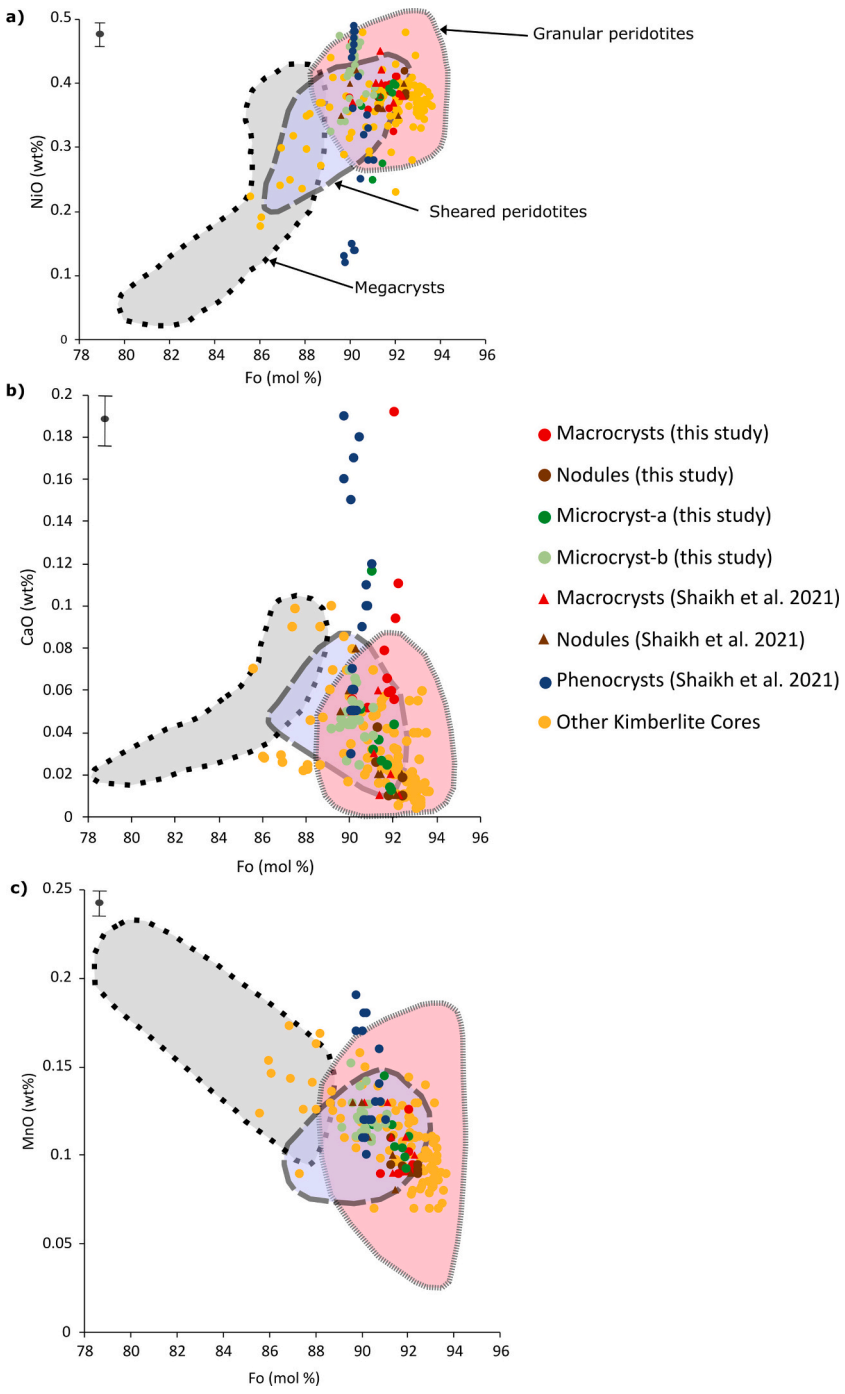

Fig. 9. Bivariate plots showing concentrations of key elements in cores of the IHV olivines and several other kimberlite olivines (consisting of literature data from Lac De Gras, Udachnaya and Kimberley, as collated in supplementary data S1). Note 'Phenocrysts' (Shaikh et al., 2021) are the equivalents of our microcrysts. Shaded red field shows granular peridotites, shaded blue field shows sheared peridotites and shaded grey field shows megacrysts (Giuliani, 2018). Error bars are representative for the original geochemical data collected in this study only. Note that the error for Fo is smaller than the data markers. (For interpretation of the references to colour in this figure legend, the reader is referred to the web version of this article.)

outermost rinds compared to other zones, with some crystals having remarkably high CaO relative to the other magmatic zones. This may indicate a substantial reduction in pressure, that is, a change in magma depth, during crystallisation of the outermost rinds - as has been noted for the olivine rims in the Lac De Gras kimberlites, Canada, which also show a wide range in CaO content of (0–0.25 wt%) (Fedortchouk and Canil, 2004). Alternatively, it may reflect late-stage fractional crystallisation of a highly evolved melt enriched in CaO, typical of kimberlites.

Again, the compositional differences between the rim, rind and outermost rind in olivines at the IHV and the respective zones in kimberlites worldwide are likely a result of assimilation during the ascent of the kimberlite melt.

4.2. Differing morphologies and zone preservations in the Igwisi Hills olivines

In terms of the grain morphology, macrocryst grains and nodules are more rounded relative to microcryst grains, which are euhedral-subhedral. The larger, macrocryst grains and nodules likely become rounded as they are more susceptible to particle-particle attrition, which

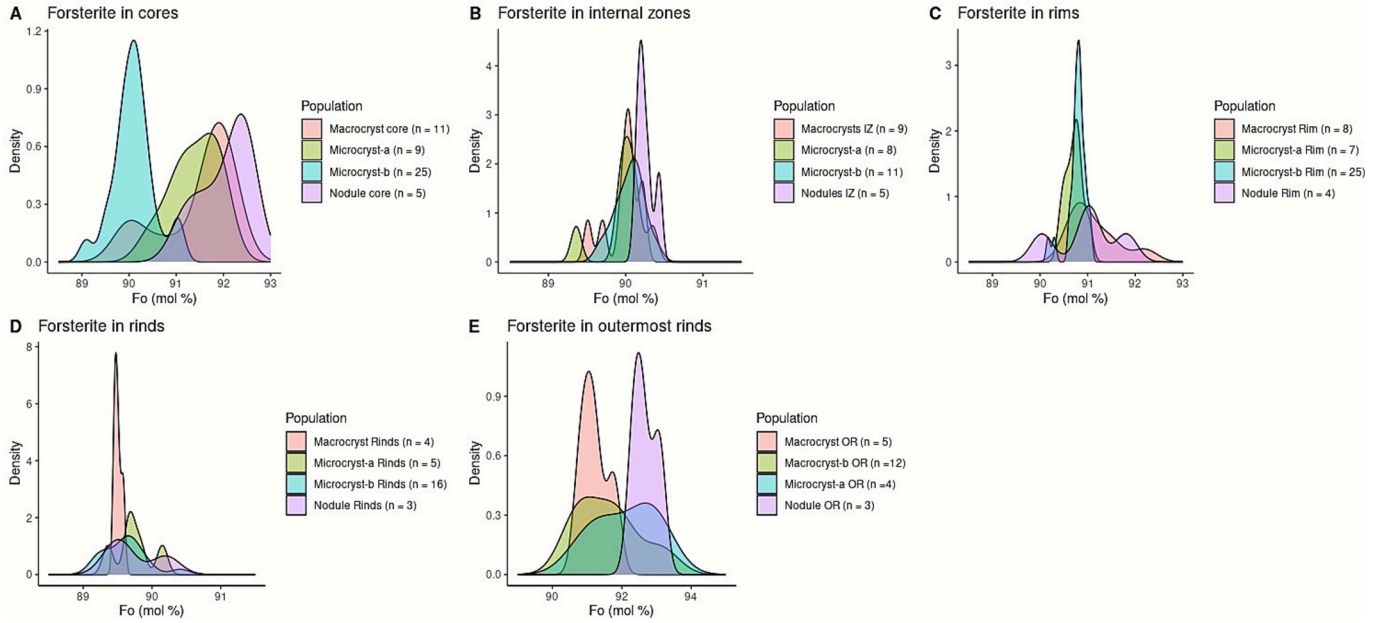

Fig. 10. Stacked density kernals of Fo contents in all 5 zones from each olivine population in the IHV lavas. Plot a) shows Fo in cores, b) Fo in internal zones, c) Fo in rims, d) Fo in rinds and e) Fo in outermost rinds. Each olivine population (macrocrysts, dunitic nodules, microcryst-a and microcryst-b are shown by a different coloured curve.

Table 2
Summary of the range of values of Fo and key oxides in macrocrysts and nodules from the Igwisi Hills lavas. Fo = forsterite in mol %. All other values are in wt% oxide. Italics denotes detection limit.

Geochemistry of macrocrysts and nodules in the Igwisi Hills lavas						
Zone	Fo	NiO	MnO	CaO	Al_2O_3	Cr_2O_3
Core	90.1–92.4	0.27–0.42	0.088–0.110	0.007–0.08	*<0.01*–0.021	*<0.008*–0.009
Internal zone	89.5–90.4	0.30–0.49	0.12–0.22	0.04–0.29	*<0.01*–0.046	*<0.008*–0.053
Rim	90.3–91.8	*<0.009*–0.37	0.14–0.33	0.1–1	*<0.01*–0.035	0.022–0.091
Rind	89.4–90.2	*<0.009*–0.18	0.2–0.25	0.21–1.24	*<0.01*–0.025	*<0.008*–0.052
Outermost rind	90.8–93.1	*<0.009*–0.058	0.22–0.32	0.25–0.57	*<0.01*–0.26	*<0.008*

Table 3
Summary of the range of values of Fo and key oxides in microcryst grains from the Igwisi Hills lavas. Fo = forsterite in mol %. All other values are in wt% oxide. Italitcs denotes detection limit.

Geochemistry of microcryst grains in the Igwisi Hills lavas						
Zone	Fo	NiO	MnO	CaO	Al_2O_3	Cr_2O_3
Microcryst-a cores	90.5–92	0.1–0.39	0.10–0.14	0.02–0.16	*<0.01*–0.008	*<0.008*–0.045
Microcryst-b cores	89–90.7	0.33–0.46	0.11–0.13	0.04–0.12	*<0.01*–0.016	*<0.008*–0.059
Internal zone	89.9–90.4	0.29–0.47	0.11–0.16	0.05–0.13	*<0.01*–0.017	*<0.008*–0.061
Rim	90.2–91.1	0.05–0.44	0.13–0.29	0.09–0.45	*<0.01*–0.037	*<0.008*–0.079
Rind	89.2–90.64	0.02–0.18	0.12–0.26	0.17–0.34	*<0.01*–0.06	*<0.008*–0.034
Outermost rind	90.8–93.25	*<0.009*–0.05	0.03–0.28	0.25–0.95	0.018–0.312	*<0.008*–0.008

is prevalent in kimberlites due to their rapid ascent and has been proposed as an important mechanism occuring during the eruption of the IHV (Jones et al., 2014; Jones and Russell, 2018). The smaller microcrysts may move upwards within the magma more freely, encountering other particles less frequently, thus more readily retaining their original, euhedral-subhedral habit. However, we see that the outer edges (10–20 um thick) of microcryst grains often have a skeletal appearance (Fig. 6) which likely reflects chemical dissolution within a rapidly evolving kimberlite melt. Furthermore, our microcryst-a grains may be more euhedral-subhedral because the magmatic zones make up the majority of each grain, with the xenocrystic cores often being very small, whereas the opposite is often true for macrocryst grains and nodules. Additionally, microcryst-a and macrocryst cores often show more extreme resorption textures compared to microcryst-b cores, indicating they are the likely most out of equilibrium with the primitive kimberlite melt.

We also observe that not all 5 archetypal zones are preserved in all the IHV olivines. In about 70 % of observed crystals, the core, internal zone and rims are preserved but there are a lack of rinds and outermost rinds. This could either reflect attrition and/or chemical dissolution of grains during rapid ascent. Alternatively, all 5 zones may simply not have formed on all olivine grains, indicating different ascent histories.

It is also worth noting that although all olivine grains seen in the IHV kimberlites appear to have similar zoning patterns, a strong bimodal size distribution of grains exist. This is a reflection of the fact that the different core types are likely sampling different mantle lithologies, as suggested by the distinct peaks for Fo in cores seen in Fig. 10,

particularly for microcryst-b grains.

4.3. Formation, evolution and ascent model for the Igwisi kimberlites

We infer a multi-stage formation process of the zones in the Igwisi Hills kimberlite olivine grains, as follows:

1) Mg-rich granular mantle peridotite grains (macrocryst, nodule and microcryst-a cores) were formed at depth.
2) Primitive kimberlite melt rose and came into contact with macrocryst, nodule and microcryst-a cores, entraining them into their flow.
3) Primitive kimberlite melt crystallises around the peridotite cores to form Fe-rich internal zones.
4) H_2O and CO_2 rich fluid/melt assisted recrystallisation of internal zones of nodules created Fe-rich neoblasts.
5) The neoblasts became disaggregated from nodules during rapid and turbulent ascent.
6) The neoblasts became cores for the microcryst-b grains.
7) As the primitive kimberlite melt ascended it evolved into a typical Ni poor, Ca rich kimberlite melt, which has elevated Fo contents indicating assimilation of Mg-rich lithosphere.
8) Archetypal, evolved kimberlite melt crystallised around the internal zones of the macrocryst, nodule and microcryst-a grains, and cores or internal zones of microcryst-b grains, to form Mg-rich rims.
9) The late stage kimberlite melt crystallised around rims of all the olivines, forming a low-Fo rind, suggesting assimilation of relatively Fe-rich lithosphere.
10) During final stages of ascent, the high-Mg outermost rind formed around all the olivines, derived from the kimberlite melt. The rise in Mg of the melt was likely due to an increase in oxygen fugacity near the surface and late stage evolution via fractional crystallisation.
11) Particularly rapid and turbulent ascent in the late stages resulted in particle-particle attrition, leading to many crystals not preserving all 5 olivine zones in the surface deposit (along with a possible influence of chemical dissolution).

5. Conclusions

We classify the olivine grains found in the Igwisi Hills kimberlite lavas into four groups, according to their size, morphology, core types, zoning patterns, Fo content and oxide geochemistry. Macrocryst grains are >1500 μm, rounded and have a high-Mg (Fo >90) resorbed xenocrystic core derived from granular mantle peridotite, surrounded by subhedral internal zones, thought to be derived from a primitive kimberlite magma which entrains the mantle peridotites. These internal zones are surrounded by thin rims with elevated Fo, rinds with depleted Fo and outermost rinds with elevated Fo all derived from the evolved kimberlite melt. Nodules have a similar size, morphology and zoning to macrocrysts but are polycrystalline, containing many small crystals called neoblasts. Microcryst-a crystals are <1500 μm, euhedral-subhedral and have a high-Mg xenocrystic core derived from granular mantle peridotite and are surrounded by primitive kimberlite melt derived internal zones and kimberlitic magmatic rims, rinds and outermost rinds which show similar Fo ranges to the same zones in macrocrysts and nodules. Microcryst-b are similar in size and morphology to microcryst-a crystals but possess an Fe-rich core interpreted to be derived from disaggregated neoblasts. They sometimes feature Fo-poor internal zones which we interpret to be derived from the primitive kimberlite melt, but these zones are not as abundant as in macrocrysts, nodules and microcryst-a grains. They also feature magmatic rims, rinds and outermost rinds with the same histories as macrocrysts, nodules and microcryst-a grains. Importantly, across all four olivine populations, not all crystals preserve all magmatic zones, likely due to particle-particle attrition during rapid, turbulent ascent. These young and well preserved kimberlite deposits at the Igwisi Hills contain olivines which show similar zoning patterns to many kimberlites worldwide. The discovery of this complex zoning in these deposits is valuable for understanding the evolution of these magmas.

CRediT authorship contribution statement

J.J. Rawlings: Data curation, Formal analysis, Investigation, Methodology, Visualization, Writing – original draft. **T.M. Gernon:** Conceptualization, Funding acquisition, Project administration, Resources, Supervision, Writing – review & editing. **M.J. Stock:** Supervision, Writing – review & editing. **M.R. Palmer:** Supervision, Writing – review & editing. **C.M. Petrone:** Supervision, Writing – review & editing. **R.J. Brown:** Resources, Writing – review & editing. **E. Humphreys-Williams:** Supervision, Writing – review & editing.

Funding

Jessica Justine Rawlings has received a PhD scholarship from NERC grant NE/S007210/1.

Declaration of competing interest

The authors declare that they have no known competing financial interests or personal relationships that could have appeared to influence the work reported in this paper.

Acknowledgements

We acknowledge John Spratt at the Natural History Museum (NHM) London for assistance with microprobe work, Richard Pearce at the University of Southampton, and Cindy Broderick and Innes Clatworthy at the NHM for their assistance with SEM work. We thank Dan Doran and Matt Beverley-Smith at the University of Southampton for sample preparation. We acknowledge funding from the INSPIRE Doctoral Training Programme under the auspices of NERC grant NE/S007210/1. We thank Hayden Dalton and an anonymous reviewer for their valuable comments which have improved this manuscript significantly.

Appendix A. Supplementary data

Supplementary data to this article can be found online at https://doi.org/10.1016/j.jvolgeores.2025.108497.

Data availability

Data will be made available on request.

References

Abersteiner, A., Kamenetsky, V.S., Goemann, K., Kjarsgaard, B.A., Rodemann, T., Kamenetsky, M., Ehrig, K., 2020. A genetic story of olivine crystallisation in the mark kimberlite (Canada) revealed by zoning and melt inclusions. Lithos 358–359. https://doi.org/10.1016/j.lithos.2020.105405. ISSN 0024-4937 https://www.sciencedirect.com/science/article/pii/S0024493720300426.

Abersteiner, A., Kamenetsky, V.S., Goemann, K., Golovin, A., Kamenetsky, M., 2022. Olivine in kimberlites: magma evolution from deep mantle to eruption. J. Petrol. 63 (7). https://doi.org/10.1093/petrology/egac055. ISSN 0022-3530.

Afonso, J.C., Salajegheh, F., Szwillus, W., Ebbing, J., Gaina, C., 2019. A global reference model of the lithosphere and upper mantle from joint inversion and analysis of multiple data sets. Geophys. J. Int. 217 (3), 1602–1628. https://doi.org/10.1093/gji/ggz094.

Arndt, N.T., Guitreau, M., Boullier, A.-M., Le Roex, A., Tommasi, A., Cordier, P., Sobolev, A., 2010. Olivine, and the origin of kimberlite. J. Petrol. 51 (3), 573–602. https://doi.org/10.1093/petrology/egp080.

Baptiste, V., Tommasi, A., Demouchy, S., 2012. Deformation and hydration of the lithospheric mantle beneath the Kaapvaal craton, South Africa. Lithos 149, 31–50. https://doi.org/10.1016/j.lithos.2012.05.001. ISSN 0024-4937. https://www.sciencedirect.com/science/article/pii/S002449371200182X.

Baranov, A.A., Bobrov, A.M., 2018. Crustal structure and properties of Archean cratons of Gondwanaland: similarity and difference. Russ. Geol. Geophys. 59 (5), 512–524. https://doi.org/10.1016/j.rgg.2018.04.005. ISSN 1068-7971. https://www.sciencedirect.com/science/article/pii/S1068797118300907.

Bassett, H., 1954. The Igwisi craters and lavas. Rec. Geol. Survey Tanganyika 4, 96–102.

Batumike, J.M., Griffin, W.L., Belousova, E.A., Pearson, N.J., Suzanne, Y.O., Shee, S.R., 2008. Lam-icpms u–pb dating of kimberlitic perovskite: eocene–oligocene kimberlites from the kundelungu plateau, D.R. CONGO. Earth Planet. Sci. Lett. 267 (3), 609–619. https://doi.org/10.1016/j.epsl.2007.12.013. ISSN 0012-821X. https://www.sciencedirect.com/science/article/pii/S0012821X07008205.

Brett, R.C., Russell, J.K., Moss, S., 2009. Origin of olivine in kimberlite: phenocryst or impostor? Lithos 112, 201–212. https://doi.org/10.1016/j.lithos.2009.04.030. ISSN 0024-4937. https://www.sciencedirect.com/science/article/pii/S0024493709001674.

Brett, R.C., Russell, J.K., Andrews, G.D.M., Jones, T.J., 2015. The ascent of kimberlite: insights from olivine. Earth Planet. Sci. Lett. 424, 119–131. https://doi.org/10.1016/j.epsl.2015.05.024. ISSN 0012-821X. https://www.sciencedirect.com/science/article/pii/S0012821X15003143.

Brown, R.J., Manya, S., Buisman, I., Fontana, G., Field, M., Niocaill, C.M., Sparks, R.S.J., Stuart, F.M., 2012. Eruption of kimberlite magmas: physical volcanology, geomorphology and age of the youngest kimberlitic volcanoes known on earth (the upper pleistocene/holocene igwisi hills volcanoes, Tanzania). Bull. Volcanol. 74 (7), 1621–1643. https://doi.org/10.1007/s00445-012-0619-8.

Bussweiler, Y., Foley, S.F., Prelević, D., Jacob, D.E., 2015. The olivine macrocryst problem: New insights from minor and trace element compositions of olivine from lac de gras kimberlites, Canada. Lithos 220-223, 238–252. https://doi.org/10.1016/j.lithos.2015.02.016. ISSN 0024-4937. https://www.sciencedirect.com/science/article/pii/S0024493715000651.

Casetta, F., Asenbaum, R., Ashchepkov, I., Abart, R., Ntaflos, T., 2023. Mantle-derived cargo vs liquid line of descent: reconstructing the p-t-fo 2 -x path of the udachnaya-east kimberlite melts during ascent in the siberian sub-cratonic lithosphere. J. Petrol. 64, 1–25. https://doi.org/10.1093/petroj/egac122.

Clifford, T., 1966. Tectono-metallogenic units and metallogenic provinces of africa. Earth Planet. Sci. Lett. 1 (6), 421–434. https://doi.org/10.1016/0012-821X(66)90039-2. ISSN 0012-821X. https://www.sciencedirect.com/science/article/pii/0012821X66900392.

Dalton, H., Giuliani, A., O'Brien, H., Phillips, D., Hergt, J., 2020. The role of lithospheric heterogeneity on the composition of kimberlite magmas from a single field: the case of Kaavi-Kuopio, Finland. Lithos 354–355. https://doi.org/10.1016/j.lithos.2019.105333. ISSN 0024-4937 https://www.sciencedirect.com/science/article/pii/S0024493719304931.

Dawson, J.B., 1971. Advances in kimberlite geology. Earth Sci. Rev. 7 (4), 187–214. https://doi.org/10.1016/0012-8252(71)90120-6. ISSN 0012-8252. https://www.sciencedirect.com/science/article/pii/0012825271901206.

Dawson, B., 1980. Kimberlites and Their Xenoliths. Springer-Verlag. https://books.google.co.uk/books?id=F0IeAQAAIAAJ.

Dawson, J.B., 1994. Quaternary kimberlitic volcanism on the tanzania craton. Contrib. Mineral. Petrol. 116 (4), 473–485. https://doi.org/10.1007/BF00310913.

Dawson, B., 2008. The Gregoy rift valley and Neogene-recent volcanoes of northern Tanzania. Geol. Soc. 1, 9 (ISBN ISBN 978-1-86239-267-0.).

De Hoog, J.C.M., Gall, L., Cornell, D.H., 2010. Trace-element geochemistry of mantle olivine and application to mantle petrogenesis and geothermobarometry. Chem. Geol. 270 (1), 196–215. https://doi.org/10.1016/j.chemgeo.2009.11.017. ISSN 0009-2541. https://www.sciencedirect.com/science/article/pii/S0009254109004677.

Fedortchouk, Y., Canil, D., 2004. Intensive variables in kimberlite magmas, lac de gras, Canada and implications for diamond survival. J. Petrol. 45 (9), 1725–1745. https://doi.org/10.1093/petrology/egh031. https://www.scopus.com/inward/record.uri?eid=2-s2.0-4544320446&doi=10.1093%2fpetrology%2fegh031&partnerID=40&md5=ea38dce8eaacb3a84500063448b3e498.

Fozzard, P.M.H., 1956. Further notes on the volcanic rocks from igwisi. Rec. Geol. Survey Tanganyika 4, 69–75.

Gernon, T.M., Jones, S.M., Brune, S., Hincks, T.K., Palmer, M.R., Schumacher, J.C., Primiceri, R.M., Field, M., Griffin, W.L., O'Reilly, S.Y., Keir, D., Spencer, C.J., Merdith, A.S., Glerum, A., 2023. Rift-induced disruption of cratonic keels drives kimberlite volcanism. Nature 620 (7973), 344–350. https://doi.org/10.1038/s41586-023-06193-3.

Gibson, S.A., McMahon, S.C., Day, J.A., Dawson, J.B., 2013. Highly refractory lithospheric mantle beneath the Tanzanian craton: evidence from Lashaine pre-metasomatic garnet-bearing peridotites. J. Petrol. 54 (8), 1503–1546. https://doi.org/10.1093/petrology/egt020.

Giuliani, A., 2018. Insights into kimberlite petrogenesis and mantle metasomatism from a review of the compositional zoning of olivine in kimberlites worldwide. Lithos 312-313, 322–342. https://doi.org/10.1016/j.lithos.2018.04.029. ISSN 0024-4937. https://www.sciencedirect.com/science/article/pii/S0024493718301567.

Giuliani, A., Pearson, D.G., Soltys, A., Dalton, H., Phillips, D., Foley, S.F., Lim, E., Goemann, K., Griffin, W.L., Mitchell, R.H., 2020. Kimberlite genesis from a common carbonate-rich primary melt modified by lithospheric mantle assimilation. Sci. Adv. 6 (17), eaaz0424. https://doi.org/10.1126/sciadv.aaz0424. https://www.science.org/doi/abs/10.1126/sciadv.aaz0424.

Giuliani, A., Schmidt, M.W., Torsvik, T.H., Fedortchouk, Y., 2023. Genesis and evolution of kimberlites. Nat. Rev. Earth Environ. 4 (11), 738–753. https://doi.org/10.1038/s43017-023-00481-2.

Giuliani, A., Dalton, H., Pearson, D.G., 2025. Kimberlites: The Deepest Geochemical Probes of Earth. Elsevier, Oxford, pp. 159–230. https://doi.org/10.1016/B978-0-323-99762-1.00064-4. ISBN 978-0-323-99763-8. https://www.sciencedirect.com/science/article/pii/B9780323997621000644.

Golovin, A.V., Sharygin, I.S., Korsakov, A.V., 2017. Origin of alkaline carbonates in kimberlites of the Siberian craton: evidence from melt inclusions in mantle olivine of the Udachnaya-east pipe. Chem. Geol. 455, 357–375. https://doi.org/10.1016/j.chemgeo.2016.10.036. ISSN 0009-2541. https://www.sciencedirect.com/science/article/pii/S0009254116305885.

Howarth, G., Gross, J., 2019. Diffusion-controlled and concentric growth zoning revealed by phosphorous in olivine from rapidly ascending kimberlite magma, Benfontein, South Africa. Geochim. Cosmochim. Acta 266. https://doi.org/10.1016/j.gca.2019.08.006.

Howarth, G.H., Taylor, L.A., 2016. Multi-stage kimberlite evolution tracked in zoned olivine from the benfontein sill, South Africa. Lithos 262, 384–397. https://doi.org/10.1016/j.lithos.2016.07.028. ISSN 0024-4937. https://www.sciencedirect.com/science/article/pii/S002449371630202X.

Jones, T.J., Russell, J.K., 2018. Attrition in the kimberlite system. Mineral. Petrol. 112 (Suppl. 2), 491–501. https://doi.org/10.1007/s00710-018-0580-0. ISSN 0930-0708 (Print) 0930-0708.

Jones, T.J., Jones, T.J., Russell, J.K., Porritt, L.A., Porritt, L.A., Brown, R.J., 2014. Morphology and surface features of olivine in kimberlite: implications for ascent processes. Solid Earth 5, 313–326.

Jones, T.J., Russell, J.K., Sasse, D., 2019. Modification of mantle cargo by turbulent ascent of kimberlite. Front. Earth Sci. 7. https://doi.org/10.3389/feart.2019.00134.

Kamenetsky, V.S., Kamenetsky, M.B., Sobolev, A.V., Golovin, A.V., Demouchy, S., Faure, K., Sharygin, V.V., Kuzmin, D.V., 2008. Olivine in the udachnaya-east kimberlite (yakutia, Russia): types, compositions and origins. J. Petrol. 49 (4), 823–839. https://doi.org/10.1093/petrology/egm033.

Kjarsgaard, B.A., de Wit, M., Heaman, L.M., Pearson, D.G., Stiefenhofer, J., Janusczcak, N., Shirey, S.B., 2022. A review of the geology of global diamond mines and deposits. Rev. Mineral. Geochem. 88 (1), 1–117. https://doi.org/10.2138/rmg.2022.88.01.

Lim, E., Giuliani, A., Phillips, D., Goemann, K., 2018. Origin of complex zoning in olivine from diverse, diamondiferous kimberlites and tectonic settings: Ekati (Canada), alto paranaiba (Brazil) and kaalvallei (South Africa). Mineral. Petrol. 112 (2), 539–554. https://doi.org/10.1007/s00710-018-0607-6.

Mitchell, R.H., 1986. Kimberlites: Mineralogy, Geochemistry, and Petrology. Springer Science and Business Media, LLC.

Mitchell, R.H., Giuliani, A., O'Brien, H., 2019. What is a kimberlite? Petrology and mineralogy of hypabyssal kimberlites. Elements 15 (6), 381–386. https://doi.org/10.2138/gselements.15.6.381.

Moore, A., Costin, G., 2016. Kimberlitic olivines derived from the CR-poor and CR-rich megacryst suites. Lithos 258-259, 215–227. https://doi.org/10.1016/j.lithos.2016.04.022. ISSN 0024-4937. https://www.sciencedirect.com/science/article/pii/S0024493716300573.

Nkere, B.J., Janney, P.E., Tinguely, C., 2021. Cr-poor and CR-rich clinopyroxene and garnet megacrysts from southern african group 1 and group 2 kimberlites: clues to megacryst origins and their relationship to kimberlites. Lithos 396–397. https://doi.org/10.1016/j.lithos.2021.106231. ISSN 0024-4937 https://www.sciencedirect.com/science/article/pii/S002449372100267X.

Pearson, D.G., Scott, J.M., Liu, J., Schaeffer, A., Wang, L.H., van Hunen, J., Szilas, K., Chacko, T., Kelemen, P.B., 2021. Deep continental roots and cratons. Nature 596 (7871), 199–210. https://doi.org/10.1038/s41586-021-03600-5.

Priestley, K., McKenzie, D., Debayle, E., Pilidou, S., 2008. The african upper mantle and its relationship to tectonics and surface geology. Geophys. J. Int. 175 (3), 1108–1126. https://doi.org/10.1111/j.1365-246X.2008.03951.x. ISSN 0956-540X. https://onlinelibrary.wiley.com/doi/abs/10.1111/j.1365-246X.2008.03951.x.

Reid, A.M., Donaldson, C.H., Dawson, J.B., Brown, R.W., Ridley, W.I., 1975. The igwisi hills extrusive "kimberlites". Phys. Chem. Earth 9, 199–218. https://doi.org/10.1016/0079-1946(75)90017-8. ISSN 0079-1946. https://www.sciencedirect.com/science/article/pii/0079194675900178.

Sampson, N.D., 1953. The volcanic hills at igwisi. Rec. Geol. Survey Tanganyika 3, 48–53.

Schulze, D. J. *Cr-Poor Megacrysts from the Hamilton Branch Kimberlite, Elliott County, Kentucky*, volume 11, pages 97–108. Elsevier, 1984. ISBN 0167-2894. doi: https://doi.org/10.1016/B978-0-444-42274-3.50015-9. URL https://www.sciencedirect.com/science/article/pii/B9780444422743500159.

Scott Smith, B.H., Nowicki, T.E., Russell, J.K., Webb, K.J., Mitchell, R.H., Hetman, C.M., Harder, M., Skinner, E.M.W., Robey, J.A., 2013. Kimberlite terminology and classification. In: Pearson, D.G., Grütter, H.S., Harris, J.W., Kjarsgaard, B.A., O'Brien, H., Rao, N.V.C., Sparks, S. (Eds.), Proceedings of 10th International Kimberlite Conference. Springer India, pp. 1–17. ISBN 978-81-322-1173-0.

Shaikh, A.M., Tappe, S., Bussweiler, Y., Vollmer, C., Brown, R.J., 2021. Origins of olivine in earth's youngest kimberlite: Igwisi hills volcanoes, tanzania craton. Contrib. Mineral. Petrol. 176 (8), 62. https://doi.org/10.1007/s00410-021-01816-2.

Shea, T., Costa, F., Krimer, D., Hammer, J.E., 2015. Accuracy of timescales retrieved from diffusion modeling in olivine: a 3d perspective. Am. Mineral. 100 (10), 2026–2042. https://doi.org/10.2138/am-2015-5163.

Simkin, T., Smith, J.V., 1970. Minor-element distribution in olivine. J. Geol. 78 (3), 304–325. https://doi.org/10.1086/627519. https://www.journals.uchicago.edu/doi/abs/10.1086/627519.

Soltys, A., Giuliani, A., Phillips, D., 2018. Crystallisation sequence and magma evolution of the de beers dyke (Kimberley, South Africa). Mineral. Petrol. 112 (2), 503–518. https://doi.org/10.1007/s00710-018-0588-5.

Soltys, A., Giuliani, A., Phillips, D., Kamenetsky, V.S., 2020. Kimberlite metasomatism of the lithosphere and the evolution of olivine in carbonate-rich melts — evidence from the Kimberley kimberlites (South Africa). J. Petrol. 61 (6). https://doi.org/10.1093/petrology/egaa062.

Sparks, R., 2013. Kimberlite volcanism. Annu. Rev. Earth Planet. Sci. 41 (1), 497–528. https://doi.org/10.1146/annurev-earth-042711-105252. https://www.annualreviews.org/doi/abs/10.1146/annurev-earth-042711-105252.

Sparks, R.S.J., Baker, L., Brown, R.J., Field, M., Schumacher, J., Stripp, G., Walters, A., 2006. Dynamical constraints on kimberlite volcanism. J. Volcanol. Geotherm. Res. 155 (1), 18–48. https://doi.org/10.1016/j.jvolgeores.2006.02.010. ISSN 0377-0273. https://www.sciencedirect.com/science/article/pii/S0377027306000588.

Tappe, S., Brand, N., Stracke, A., Acken, D., Liu, C.-Z., Strauss, H., Wu, F.-Y., Luguet, A., Mitchell, R., 2016. Plates or plumes in the origin of kimberlites: U/pb perovskite and Sr-Nd-Hf-Os-C-O isotope constraints from the superior craton (Canada). Chem. Geol. 455. https://doi.org/10.1016/j.chemgeo.2016.08.019.

Tomlinson, E.L., Kamber, B.S., 2021. Depth-dependent peridotite-melt interaction and the origin of variable silica in the cratonic mantle. Nat. Commun. 12 (1), 1082. https://doi.org/10.1038/s41467-021-21343-9.

Tovey, M., Giuliani, A., Phillips, D., Nowicki, T., Pearson, D.G., Fedortchouk, Y., Russell, J.K., 2022. Controls on the emplacement style of coherent kimberlites in the lac de gras field, Canada. J. Petrol. 63 (4). https://doi.org/10.1093/petrology/egac028.

Wang, Z., Kusky, T., Fu, J., Yuan, Y., Zhu, P., 2016. Review of lithospheric destruction in the North China, North Atlantic, and tanzanian cratons. J. Geol. 124, 699–721. https://doi.org/10.1086/688608.

Willcox, A., Buisman, I., Sparks, R.S.J., Brown, R.J., Manya, S., Schumacher, J.C., Tuffen, H., 2015. Petrology, geochemistry and low-temperature alteration of lavas and pyroclastic rocks of the kimberlitic igwisi hills volcanoes, Tanzania. Chem. Geol. 405, 82–101. https://doi.org/10.1016/j.chemgeo.2015.04.012. ISSN 0009-2541. https://www.sciencedirect.com/science/article/pii/S0009254115002004.

Wilson, L., Head, J.W., 2007. An integrated model of kimberlite ascent and eruption. Nature 447 (7140), 53–57. https://doi.org/10.1038/nature05692.